Available online at www.sciencedirect.com
SCIENCE DIRECT®
Journal of Fluorine Chemistry 125 (2004) 1703–1707
JOURNAL OF FLUORINE CHEMISTRY
www.elsevier.com/locate/fluor

Graphite intercalation chemistry with large fluoroanions

Wei Yan[a], Lyuba Kabalnova[a], Nipaka Sukpirom[b], Sherry Zhang[c], Michael Lerner[a,*]

[a]Department of Chemistry, Oregon State University, Gilbert Hall, Corvallis, OR 97331, USA
[b]Department of Chemistry, Faculty of Science, Chulalongkorn University, Bangkok 10330, Thailand
[c]Lawrence Berkeley Labs, Mail Stop 2-100, 1 Cyclotron Road, Berkeley, CA 94720, USA

Available online 5 November 2004

Abstract

The syntheses and structures of graphite intercalations compounds (GIC's) containing perfluoroalkylimide, perfluoroalkylsulfonate, or perfluoroalkylborate ester anions are described. Synthetic methods include both chemical oxidation, typically performed using K_2MnF_6 in concentrated hydrofluoric or hydrofluoric/nitric acids, and electrochemical oxidation using a nitromethane-based electrolyte. These large fluoroanions generate larger and more complex intercalate galleries than are generally known for GIC's. The anion packing effects on intercalate orientation and conformation is described.

Keywords: Graphite; Intercalation; Fluoroanions; X-ray diffraction

1. Introduction

Graphite can be either oxidized or reduced to form graphite intercalation compounds (GIC's) [1]. Upon oxidation, anions intercalate between the sheets, expanding the lattice along the stacking direction. Intercalation proceeds with long-range ordering in the sequence of expanded galleries—this phenomenon is known as staging. Stage 1 is the most highly oxidized phase, where intercalate occupies galleries between all graphene sheets; Stage 2 has alternate galleries occupied; Stage 3 has every third gallery occupied, and etc. This long-range intercalate ordering allows energy minimization and results from the mechanical flexibility of the graphene sheets [2].

One challenging aspect in these intercalation reactions is the high potential required for graphite oxidation. The onset potential for intercalation typically exceeds 4 V versus Li/Li^+, with increasing potentials as oxidation continues to lower stage GIC's. These high potentials limit the methodologies and reagents that can be used to as intercalate anions and neutral molecules between graphene sheets.

Nevertheless, oxidized GIC's have been prepared with many types of oxidatively-stable intercalate anions, including tetrahedral or octahedral fluoro-, chloro-, bromo- or oxometallates [3,4], trifluoroacetate [5], perfluoroalkyl-substituted sulfonyl imides or methides [6,7], and perfluoroalkylsulfonates [8–11]. The gallery expansions in forming these GIC's range from ≈3.4 Å for graphite bifluoride, C_xHF_2 and graphite nitrate, C_xNO_3, to ≈22 Å for $C_xC_8F_{17}SO_3$ [10]. The intercalation of large anions, with highly expanded galleries, can be a first step in exploring a broader range of opportunities in graphite chemistry for selective sorption, catalysis, and nanocomposite assembly.

The first and smallest perfluoroalkylsulfonate intercalate, $CF_3SO_3^-$, yields a gallery expansion of 4.7 Å, which is consistent with a monolayer arrangement of intercalate anions. Electrochemical oxidation of graphite with perfluoroalkylsulfonates $C_nF_{2n+1}SO_3^-$ ($n = 4, 6, 8$) produces GIC's with a bilayer arrangement of anion intercalates.[8–11] A chemical method has also been employed to obtain new GIC's containing perfluoroalkylimides and the methide $C(SO_2CF_3)_3^-$ [11]. The chemical method easily generates multi-gram quantities and requires no binders or additives; this combined with the ambient stability of these products allows a more detailed structural analysis from relatively high-quality powder X-ray diffraction (PXRD) data. As an

* Corresponding author. Tel.: +1 541 737 2081; fax: +1 541 737 2062.
E-mail address: michael.lerner@orst.edu (M. Lerner).

0022-1139/$ – see front matter © 2004 Elsevier B.V. All rights reserved.
doi:10.1016/j.jfluchem.2004.09.007

example, the degree of helical twisting of fluorocarbon chains in the intercalate layer in $C_xC_8F_{17}SO_3$ was examined previously [11].

This paper reviews recent results in the chemical intercalation of the perfluoroalkylsulfonate anions $C_{10}F_{21}SO_3^-$, $C_2F_5OC_2F_4SO_3^-$ and $C_2F_5(C_6F_{10})SO_3^-$; and two perflouroalkyl chelate borates, ($B[OC(CF_3)_2C(CF_3)_2O]_2^-$) [12] and $B[OC(CF_3)_2C(O)O]_2^-$ [13]. The GIC's obtained are mainly characterized by PXRD, with structural models obtained by fitting one dimensional electron density maps to observed data.

2. Results and discussion

2.1. Graphite borates

The potential-charge curve obtained by electrochemical intercalation of $B[OC(CF_3)_2C(CF_3)_2O]_2^-$ shows a series of plateaus and ascending regions characteristic of graphite intercalation (Fig. 1, line i). The potential increases when a single phase is present, the voltage plateaus indicate the conversion of one stage into another—during oxidation this means the higher stage converted to the lower stage. For comparison, Fig. 1 also provides a charge curve for $LiN(SO_2CF_3)_2/CH_3NO_2$ [14] with the same electrolyte solvent and salt concentration employed.

The GIC stage and gallery height at each labeled transition point in these galvanostatic charge curves was determined by ex situ PXRD data from the graphite electrodes; these are reported in Table 1.

Although the shapes and GIC stages for these different anions are similar, the potentials at the transition points differ significantly. The small difference in charge required to reach these transition points is very likely due to different current efficiencies for the two electrolytes. This is associated with a slightly different oxidation potential for the two borate anions.

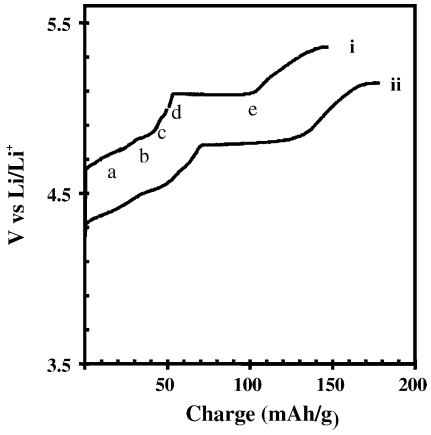

Fig. 1. Galvanostatic potential–charge curves for graphite electrodes oxidized in: (i) 0.3 M $NaB[OC(CF_3)_2C(CF_3)_2O]_2/CH_3NO_2$ at a rate of 10 mA/g; and (ii) 0.3 M $LiN(SO_2CF_3)_2/CH_3NO_2$ at a rate of 50 mA/g.

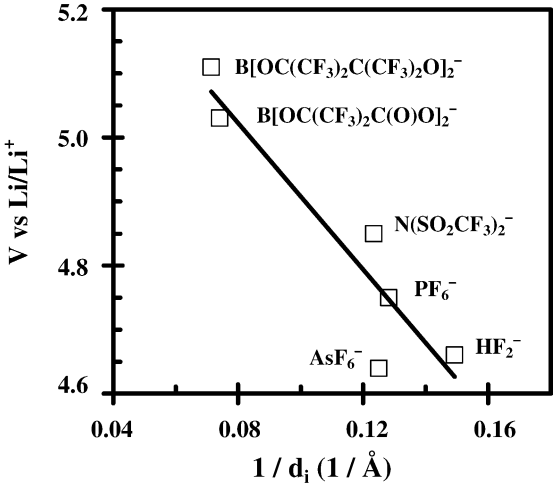

Fig. 2. Relationship between oxidation potential for Stage 2 GIC's and $1/d_i$.

Fig. 2 shows a plot of the potentials for the Stage 2 GIC's versus $1/d_i$, where d_i is the gallery height, for several GIC's. In a simple energetic model, lattice enthalpies for two-dimensional ionic structures are inversely proportional to the separation of ionic charges. The approximately linear relation in Fig. 2 confirms the utility of this simple model, and thus explains the high potentials required for intercalation of the larger $B[OC(CF_3)_2C(CF_3)_2O]_2^-$ and $B[OC(CF_3)_2C(O)O]_2^-$ anions. Some anions do not fall very close to this linear relation (note, for example, AsF_6^- in Fig. 2), this might arise from experimental differences or some GIC structural details; nevertheless, the general agreement suggests the simple model is a useful starting point. Extrapolation to very large d_i suggests that electrolytes stable to >5.2 V versus Li/Li^+ are necessary to obtain highly separated graphene layers or single-sheet graphene layer colloids layers.

The geometry-optimized structural model for $C_xB[OC(CF_3)_2C(CF_3)_2O]_2$ is shown in Fig. 3. Intercalate anions in GIC's normally adopt orientations to minimize gallery heights, this results in the minimal separation of positive sheet charges and anion centers. For large or asymmetric intercalates, however, packing effects must also

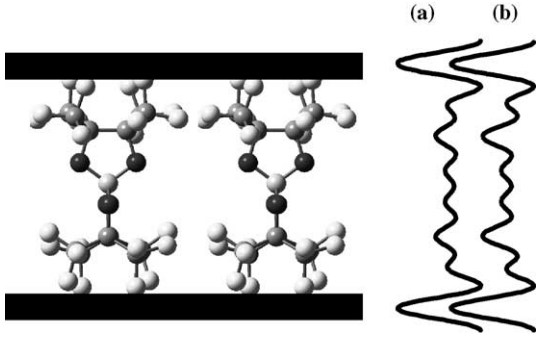

Fig. 3. One-dimensional electron density map generated from this structural model (a) closely agrees with that derived from the observed PXRD peak intensities (b).

Table 1
Stage (gallery height in Å) for GIC's obtained by electrochemical methods with chelate borate anions

Intercalate anion	Transition point in charge curve				
	a	**b**	**c**	**d**	**e**
$B[OC(CF_3)_2C(O)O]_2^-$	4 (13.3)	3 (13.7)	2 (13.8)	2 (13.9)	2 (13.9)
$B[OC(CF_3)_2C(CF_3)_2O]_2^-$	4	3 (14.0)	2	2 (14.3)	1 (14.2)

The potential charge plot for $B[OC(CF_3)_2C(CF_3)_2O]_2^-$ is shown in Fig. 1.

be considered. The orientation shown, with borate anions "standing" in galleries, requires a smaller "footprint" on the graphene layer surface, and therefore allows high charge densities within each intercalate gallery. Steric models indicate that these anions would require $x > 72$ for a "lying down" orientation in a Stage 2 GIC (where x is the ratio of graphene C atoms/anion), while a common value for small anions is $x = 48$ [15].

As with other GIC's with anions containing a high perfluoroalkyl group content, $C_xB[OC(CF_3)_2C(CF_3)_2O]_2$ is relatively stable against reduction under ambient conditions. Decomposition occurs slowly according to:

$$C_xAn + \tfrac{1}{2}H_2O \rightarrow \text{higher stage GIC} \rightarrow C_x + \tfrac{1}{4}O_2 + HAn \quad (1)$$

The observed stability appears to be related to the formation of a passivation layer at the GIC surface. Some of these GIC's are stable for days or weeks under ambient conditions [16].

2.2. Graphite perfluoroalkylsulfonates

GIC's were obtained with $C_{10}F_{21}SO_3^-$, $C_2F_5OC_2F_4SO_3^-$ and $C_2F_5(C_6F_{10})SO_3^-$ anion intercalates by a chemical method in a hydrofluoric/nitric acid solution. A schematic model of the anion bilayers is shown in Fig. 4, the sulfonate headgroups in each anion layer lie opposite the positive graphene sheet surfaces, with fluorocarbon groups extending into the gallery centers.

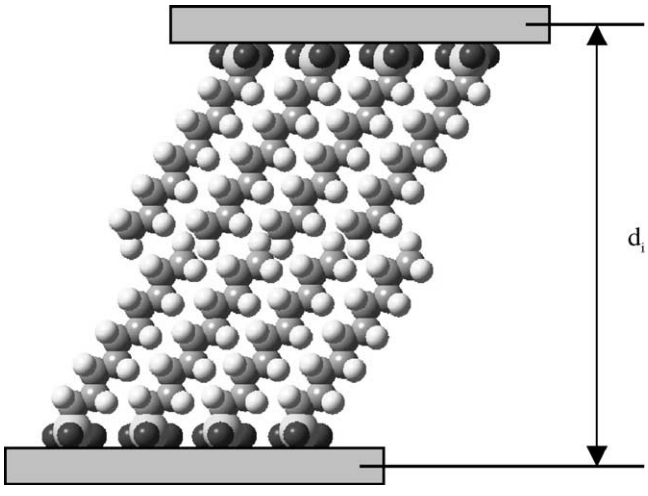

Fig. 4. Schematic diagram of Stage 2 $C_xC_{10}F_{21}SO_3$, indicating the anion bilayer structure and intercalate orientation within galleries.

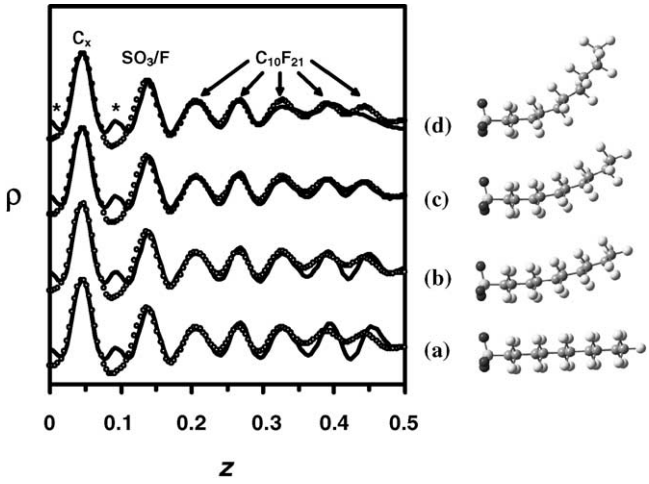

Fig. 5. Electron density maps for $C_{10}F_{21}SO_3^-$ linear anion (a), and with dihedral angles = 5° (b), 8° (c), and 15° (d). Open circles are from PXRD data, solid lines calculated from structure models. Asterisks show second-order peaks from the graphene plane.

Observed and calculated electron density maps for the $C_{10}F_{21}SO_3^-$ anion intercalate conformation are shown in Fig. 5, and for the $C_2F_5(C_6F_{10})SO_3^-$ anion intercalate in Fig. 6.

The peaks labeled SO_3/F in Figs. 5 and 6 indicate the position of the anion SO_3 headgroups; these groups orient with the O plane parallel to the graphene layer. The structure models and chemical analyses indicate that additional F, as fluoride or bifluoride, is also present at a similar distance from the graphene sheets. For each anion, the fluorocarbon

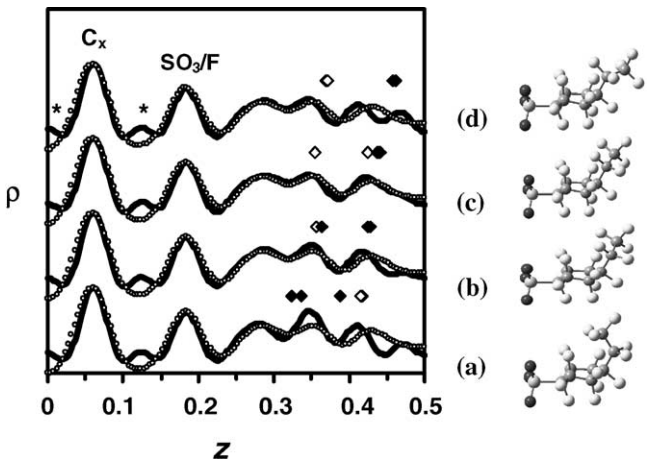

Fig. 6. Electron density maps for $C_2F_5(C_6F_{10})SO_3^-$. Conformations shown are optimized isolated anion (a), and ring-C_2F_5 rotation angle = 90° (b), 100° (c), and 135° (d). Open circles are from PXRD data; solid lines are calculated. Asterisks show second-order peaks from the graphene plane. Open and solid diamonds show F atom positions in the pendant $-C_2F_5$ group.

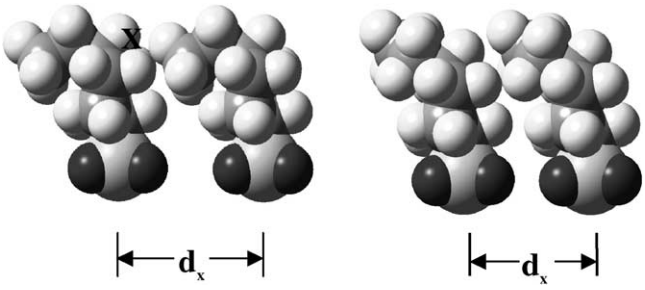

Fig. 7. Illustration of anion closest approaches for $C_2F_5(C_6F_{10})SO_3^-$ conformations with different orientations of the pendant $–CF_2CF_3$ group. Rotation of the terminal $–CF_3$ away from the ring allows denser anion packing.

peaks are fit by adopting a single additional structural parameter that modifies anion conformations. For $C_xC_{10}F_{21}SO_3$, the best fit indicates a helical fluorocarbon chain with dihedral angle ≈8°. For $C_xC_2F_5(C_6F_{10})SO_3$, the best fit indicates a rotation of the C–CF_3 bond by ≈100° towards the gallery center. The anion conformation in this GIC is, therefore, changed markedly from the isolated anion calculation, with the $–CF_3$ group moved inwards towards the gallery center.

In both of these cases, the observed conformational changes can be related to the steric requirements of intercalate packing. From space-filling models, the closest approach of different $C_2F_5(C_6F_{10})SO_3^-$ conformations in an anion bilayer was determined as shown in Fig. 7. The two illustrations show the decrease in anion footprint upon rotation of the C–C bond to orient the $–CF_3$ away from the SO_3 headgroup, calculations indicate an increased packing efficiency of 12%. This represents an unusual case for GIC's, where intercalate conformation changes are related to packing requirements.

3. Conclusion

The electrochemical oxidation of graphite to intercalate $(B[OC(CF_3)_2C(CF_3)_2O]_2^-$ produces Stages 1–3 GIC's. As with other GIC's containing large perfluoroanions, these materials can be prepared in aqueous acid and are relatively stable to prolonged exposure to ambient environment. The structures of this new GIC, and that with $B[OC(CF_3)_2C(O)O]_2^-$, have the intercalate anions oriented in a monolayer arrangement with gallery heights of 13.3–13.9 Å. These anions, therefore, adopt a ''standing-up'' anion orientation within galleries. Again, the unusual gallery structure is discussed in terms of anion footprint and efficient intercalate packing within galleries. A generally linear relation of intercalation potential to reciprocal of GIC gallery height can be related to a simple energetic model.

Stage 2 GIC's with three perfluoroalkylsulfonate anions, $C_{10}F_{21}SO_3^-$, $C_2F_5OC_2F_4SO_3^-$ and $C_2F_5(C_6F_{10})SO_3^-$ are prepared by chemical oxidation and the structures described in detail. Structural information is derived by modeling one dimensional electron density maps obtained via powder diffraction data. These structure models provide the anion concentrations, orientations, and conformations in the intercalate galleries. In all these materials, anion bilayers are observed with anion sulfonate headgroups oriented towards the graphene sheets. The intercalate anion conformations are different than those calculated or observed for the isolated or fully solvated anions. Changes in dihedral angles, involving rotations about C–C or C–O bonds, are observed for the anion intercalates, and the structural changes observed are correlated with more efficient packing of these large anions within the galleries.

4. Experimental details

GIC's were all prepared by either chemical or electrochemical oxidation methods that have been described previously [7,10–12]. In a typical chemical reaction, a Stage 2 $C_xC_{10}F_{21}SO_3$ was obtained in an ambient environment by stirring graphite powder (10 mmol) into a 30 mL solution of K_2MnF_6 (2 mmol) and $C_{10}F_{21}SO_3K$ (1 mmol) in 48% HF/69% HNO_3 (70/30, v/v). After 72 h, the product was filtered and rinsed with 48% HF followed by hexane, then dried in vacuo for 24 h. Electrochemical oxidations were performed under an Ar/He atmosphere at ambient temperature using a two-compartment cell containing a glass-frit separator. A typical electrolyte solution was 0.3 M $NaB[OC(CF_3)_2C(CF_3)_2O]_2$ in CH_3NO_2. Cells employed a lithium metal reference electrode. Working electrodes were prepared by painting a slurry of graphite and inert polymer binder in cyclohexane onto Pt mesh and drying to remove solvent, as reported previously. Galvanostatic oxidations were carried out at lower current densities, approximately 10 mA/g. After the electrochemical preparations, working electrodes were dried to remove residual liquid electrolyte at 100 mTorr.

Powder X-ray diffraction (PXRD) data were collected on a Siemens D5000 diffractometer using Ni-filtered Cu Kα radiation (1.5418 Å). A variable slit mode was used; with the detector slit width set to 0.2 mm. Data were collected from $2\theta = 2°$ to 60° in 0.02° steps, counting for 9.6 s per step.

Optimal geometries for isolated anions were calculated using the hybrid density functional method (B3LYP) with a 3–21G* basis set and GAUSSIAN 98W software. For some anions, subsequent optimization to fit the diffraction results was carried out using the PM3 model and SPARTAN 02 software. One-dimensional electron density maps were generated from both the observed PXRD data sets and the calculated structure models. Structure factors were obtained from the experimental data using:

$$F_{obs}(0\,0\,l) = \pm[I/(1+\cos^2 2\theta)/(\sin^2\theta\cos\theta)]^{1/2} \quad (2)$$

where l is the Miller index and I is the observed integrated peak intensity. Structure models were assumed to adopt

centrosymmetric unit cells; hence, the structure factors were calculated using:

$$F_{\mathrm{cal}}(0\,0\,l) = \sum_{i=1}^{n} 2f_i \cos(2\pi l z_i) \quad (3)$$

where f_i is the angle-dependent scattering factor [17], z_i is the fractional coordinate along z, and n corresponds to half of the total atoms in the unit cell. Electron density maps were generated from $z = 0$–0.5 at increments of $0.004z$ using:

$$\rho(z) = \frac{1}{c}\left[F_0 + 2\sum_{l=1}^{m} F_{0\,0\,l} \cos(2\pi l z)\right] \quad (4)$$

where c is the unit cell dimension, F_0 is the zero order structure factor, and m is the number of observed reflections. Structural refinement involved minimization of the crystallographic R factor.

Acknowledgements

The authors gratefully acknowledge support from NSF grant DMR-9900390, and Professor Kevin Gable (OSU Chemistry) for helpful discussions.

References

[1] N. Bartlett, B.W. McQuillan, Graphite chemistry, in: M.S. Whittingham, A.J. Jacobsen (Eds.), Intercalation Chemistry, Academic Press, New York, 1982, pp. 19–53.
[2] H. Zable, S.A. Solin (Eds.), Graphite Intercalation Compounds, vol. 1, Springer–Verlag, Berlin, 1990.
[3] E. Stumpp, Mater. Sci. Eng. 31 (1977) 53–59.
[4] M. Dresselhaus, G. Dresselhaus, Adv. Phys. 30 (1981) 139–226.
[5] E. Bourelle, J. Douglade, A. Metrot, Mol. Cryst. Liq. Cryst. A 244 (1994) 227–232.
[6] X. Zhang, N. Sukpirom, M. Lerner, Mater. Res. Bull. 34 (1999) 363–372.
[7] X. Zhang, M. Lerner, Mol. Cryst. Liq. Cryst. A 340 (2000) 37–42.
[8] D. Horn, H.P. Boehm, Mater. Sci. Eng. 31 (1977) 87–89.
[9] H.P. Boehm, W. Helle, B. Ruisinger, Synth. Met. 23 (1988) 395–400.
[10] Z. Zhang, M. Lerner, Chem. Mater. 8 (1996) 257–263.
[11] X. Zhang, M. Lerner, Chem. Mater. 11 (1999) 1100–1109.
[12] W. Yan, M. Lerner, J. Electrochem. Soc. 150 (2003) D169–D173.
[13] W. Yan, M. Lerner, J. Electrochem. Soc. 151 (2004) J15–J20.
[14] W. Yan, M. Lerner, J. Electrochem. Soc. 148 (2001) D83–D87.
[15] D. Billaud, A. Chenite, J. Power Sources 13 (1984) 1–7.
[16] X. Zhang, M. Lerner, H. Gotoh, M. Kawaguchi, Carbon 38 (2000) 1775–1783.
[17] Z. Su, P. Coppens, Acta Cryst. A 53 (1997) 749–762.